Meteorol. Appl. 4, 317–324 (1997)

The dry intrusion perspective of extra-tropical cyclone development

K A Browning, *Joint Centre for Mesoscale Meteorology, Department of Meteorology, University of Reading, P O Box 243, Reading, RG6 6BB, UK*

The dry intrusion is a coherent region of air descending from near tropopause-level. It often has a clear signature in satellite imagery, especially in the water vapour channel, where it is seen as a 'dark zone'. Parts of dry intrusions are characterised by high potential vorticity and, upon approaching a low-level baroclinic zone, rapid cyclogenesis may be expected to ensue. The leading edges of dry intrusions are defined by cold θ_w-fronts (moisture fronts). In some places the dry intrusion undercuts rearward-ascending warm air to give an ana-cold front. In other places it overruns the warm air to produce an upper cold θ_w-front in advance of the surface cold front. Here the dry intrusion is associated with the generation of potential instability and its eventual release as showers or thunderstorms. Identification of dry intrusions provides the forecaster with additional nowcasting evidence that is especially helpful when issuing severe weather warnings. The identification of water vapour dark zones associated with dry intrusions can also form the basis of methods for validating NWP models. Through their relationship to high potential vorticity, they can provide guidance for bogussing NWP models in situations of potentially severe weather. This article provides an introduction to the structure and behaviour of dry intrusions and their relationship to other aspects of extra-tropical cyclones.

1. Introduction

In considering the structure of cyclones it is natural to think first in terms of moist ascent and cloud: after all, we know that latent heating plays a major role in cyclogenesis. Yet this is only half the picture. In this article we focus instead on the very dry air which often comes down to low levels near cyclones. Although re-ascending in places close to the cyclone centre, this air will normally have had a long history of descent, the driest parts having been close to the tropopause upstream two days earlier. This is portrayed vividly in Figure 1, which was drawn as long ago as 1964 by the meteorologist-cum-artist E. F. Danielsen.

Danielsen's visualisation shows trajectories of cold dry air descending within a three-dimensional isentropic surface. The trajectories originate from the vicinity of a newly developing tropopause fold (i.e. a region of locally lowered tropopause) and they then fan out as they descend toward the ground behind the cold front. Analyses by Wernli (1995) suggest that some of the cyclonic trajectories originate within the stratosphere but that most of them probably originate just on the tropospheric side of the fold. The exact configuration of these dry-air trajectories varies from case to case. Thorncroft *et al.* (1993) have defined two archetypes in which either the cyclonic or the anticyclonic flow predominates depending on whether the ambient zonal shear is cyclonic or anticyclonic.

As discussed in section 3, some of this dry air undercuts warm air ahead of it whilst another portion of the dry airstream closer to the cyclone centre overruns the warm air to produce a distinctly different frontal structure. The term dry intrusion is sometimes used broadly to refer to the entire dry flow in Figure 1 and sometimes more restrictively to focus on the overrunning portion. Two particularly important properties of the

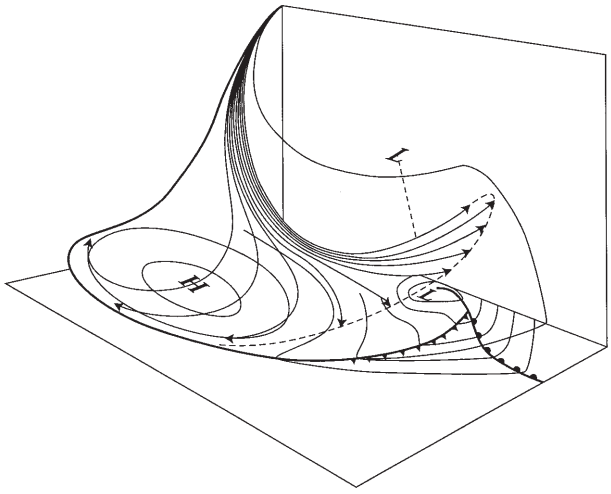

Figure 1. *Three-dimensional representation of the dry intrusion flow. Arrows are trajectories of air originating from a small region near the tropopause, drawn within a curved isentropic surface. These trajectories come close to the ground in the left part of the diagram but not in the right-hand part, where they overrun the surface fronts (Danielsen, 1964).*

dry intrusion are the high potential vorticity (PV) of parts of it and the low wet-bulb potential temperature (θ_w) of other parts The effect the high PV has in promoting cyclogenesis is discussed in section 5 and the effect the low θ_w has in generating potential instability and convection is discussed in sections 4 and 6.

The identification of the dry intrusion as a significant entity associated with cyclone development has come to prominence through its association with characteristic signatures in satellite imagery. After the onset of cyclogenesis the dry intrusion can be seen as a so-called 'dry slot' in the water vapour (WV), infra-red (IR) and, sometimes, in the visible (VIS) channel. As shown in Figure 2 the dry slot is the relatively cloud-free region sandwiched between a high-topped polar-front cloud band on one side and an often slightly lower cloud feature, known as a cloud head, on the cold-air side. We elaborate on the relationship of the dry intrusion to the airflows in these cloudy regions in section 2.

Prior to the development of the dry slot (i.e. before it is flanked on both sides by cloud), the dry intrusion is not evident in the IR or VIS imagery. However, the dry intrusion is often evident in the WV imagery up to a day before it is detected in the IR and VIS; it is seen in the WV imagery during this period as an expanding 'dark zone' (Smigielski & Ellrod, 1985; Young *et al.*, 1987; Weldon & Holmes, 1991). An example is shown later in Figure 10. The precise shape of a WV dark zone varies depending on factors such as the shape of the trough–ridge system.

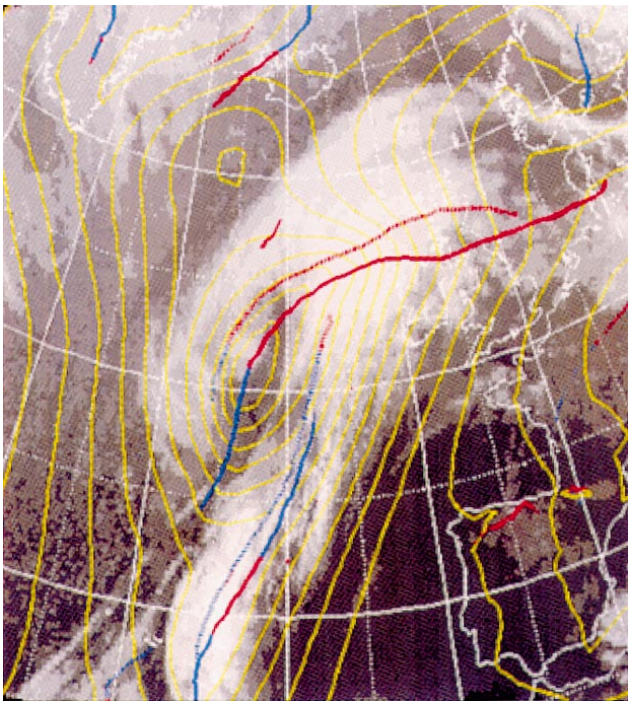

Figure 2. *Meteosat infra-red image for 2100 UTC on 7 October 1995 showing a dry slot sandwiched between a polar-front cloud band to the southeast and a cloud head to the northwest. Superimposed is the three-hour forecast from the operational Met. Office Limited Area Model as produced routinely using the method outlined by Hewson (1997) in this issue. Yellow lines are sea-level isobars. Red and blue lines are objectively derived warm and cold fronts, respectively. Surface fronts are shown solid and upper (600 mb) fronts are dotted, thereby enabling the slope of the fronts to be visualised in relation to the cloud pattern.*

2. Relationship of the dry intrusion to moist ascending air

The dry intrusion can be visualised to a zeroth order approximation as one half of a rather symmetrical transverse circulation, as shown in Figure 3. As the descending dry-intrusion air fans out behind the surface cold front, the ascending moist flow fans out in the middle or upper troposphere behind a front-like boundary corresponding to the convex outer edge of the cloud head. The two flows intertwine in the region of the cyclone centre (L) where part of the dry intrusion (with low θ_w) overrides part of the moist flow (high θ_w). The leading edge of the overrunning part of the dry intrusion constitutes an upper- or middle-level cold θ_w-front (moisture front), often referred to simply as an upper cold front (UCF). Depending on the magnitude of the ambient stretching deformation, the two fan-shaped flows may be elongated parallel to the cold front more or less than that shown in Figure 3.

Analysts concerned with interpreting satellite imagery for research (Browning & Roberts, 1994) and opera-

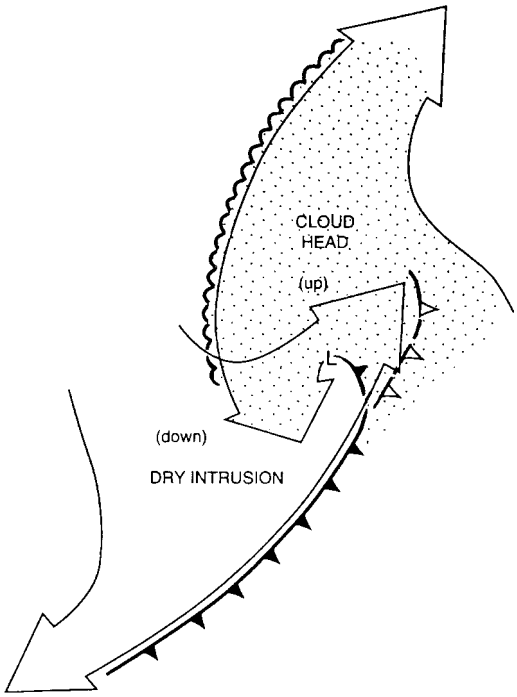

Figure 3. *Highly idealised conceptual model showing the intertwining around the cyclone centre (L) of two rather symmetrical flows: the dry intrusion and a moist flow responsible for the cloud head (originating from both sides of the warm front as clarified in Figure 4). The leading edge of much of the dry intrusion is situated along a surface cold front. Part of the dry intrusion overruns the moist flow to give an upper cold front (open frontal symbols). (After Browning* et al., *1995.)*

tional forecasting purposes (Bader *et al.*, 1995) have refined the model in Figure 3. They have concentrated on defining the moist flows in terms of so-called conveyor-belt flows. Figure 4 shows the cloud-head flow in Figure 3 to be made up partially of a cold-conveyor-belt (CCB) flow originating ahead of the surface warm front. This is overridden by a flow originating from the warm sector, referred to as a secondary warm conveyor belt (W2). It is the latter, high θ_w , flow that is itself overrun by the low θ_w dry intrusion to produce the potential instability responsible for the convective events as discussed in section 4.

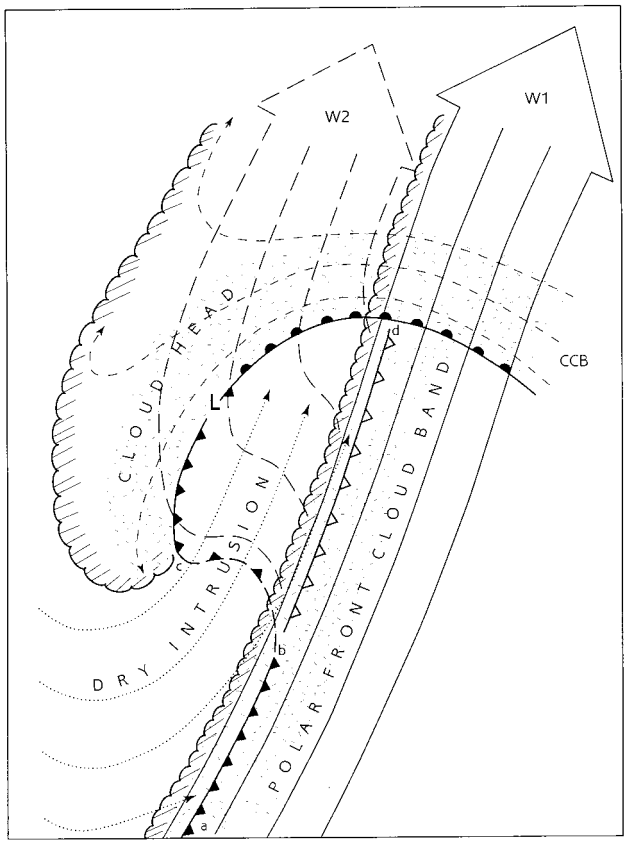

Figure 4. *Structure of a developing extratropical cyclone (confluent-flow type). The cyclone centre (L) is travelling towards the top right. The surface warm front is shown conventionally. Part of the bent-back front (cd) is plotted as a cold front with closely spaced frontal symbols. The main surface cold front (ab) is shown similarly. In between the two sharp surface cold fronts (bc) there is a diffuse surface cold front drawn dashed with widely spaced frontal symbols. The cold front drawn with open symbols (bd) is an upper cold θ_w-front (UCF) marking the edge of the dry intrusion. Principal airflows, drawn relative to the system, are: the main warm conveyor belt (W1) (solid lines), the secondary warm conveyor belt (W2) (long-dash lines), the cold conveyor belt (CCB) (short-dash lines) and the dry intrusion (dotted lines). The cold-air sides of the main cloud features are drawn scalloped and hatched: the polar-front cloud band is due to W1, and the cloud head is due to the combined effect of W2 and the CCB. Precipitation (stippled areas) reaches the surface along the left side of W1, near the cold fronts, and above the warm frontal zone; precipitation also falls from the inner parts of the cloud head starting at the bent-back front. The two main areas of precipitation are separated by a dry slot where the shallow W2 flow (shallow moist zone) is capped by the dry intrusion. The dry slot is usually characterised by partial shallow cloudiness.*

Also shown in Figure 4 is a major flow of high θ_w air labelled W1. This is the primary warm conveyor belt (WCB) responsible for the polar-front cloud band which for simplicity was omitted from Figure 3. This flow and its associated cloud shield deepens as it travels towards, and eventually rises above, the warm frontal zone. Its left-hand boundary is often sharply defined in the satellite imagery where it encounters dry-intrusion air undercutting it, sometimes to a greater degree than shown in Figure 4.

The overall situation depicted in Figure 4 corresponds to the frontal-fracture stage of Shapiro & Keyser's (1990) cyclone life-cycle model. However, the precise configuration of the principal flows depends on the larger-scale ambient flow (Bader *et al.*, 1995). We shall confine ourselves here to drawing a contrast between two major archetypes identified by Young (1994). The first of these, corresponding to Figure 4, occurs in association with confluent troughs. The second common archetype, shown in Figure 5, occurs in association with diffluent troughs. Here, the secondary WCB extends to a greater distance away from the primary WCB before rising in the cloud head, and it is overrun by dry-intrusion air over a broader front.

3. Relationship of the dry intrusion to the cold frontal structure

Figure 6 shows a Met. Office Limited-Area Model portrayal of the dry intrusion for a case conforming to the diffluent-trough archetype in Figure 5. Over the previous nine-hour period the cloud head had emerged

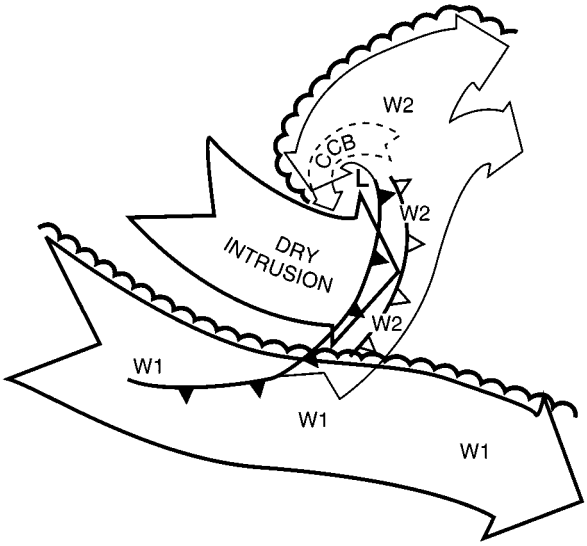

Figure 5. *Conceptual model showing system-relative airflow associated with the diffluent-flow type of cyclogenesis. The arrows labelled W1 and W2 are the primary and secondary warm conveyor belts. The dashed arrow labelled CCB is a cold conveyor belt. The dry intrusion is seen to overrun W2 over a broad region to produce an upper cold front at its leading edge. (After Young, 1994.)*

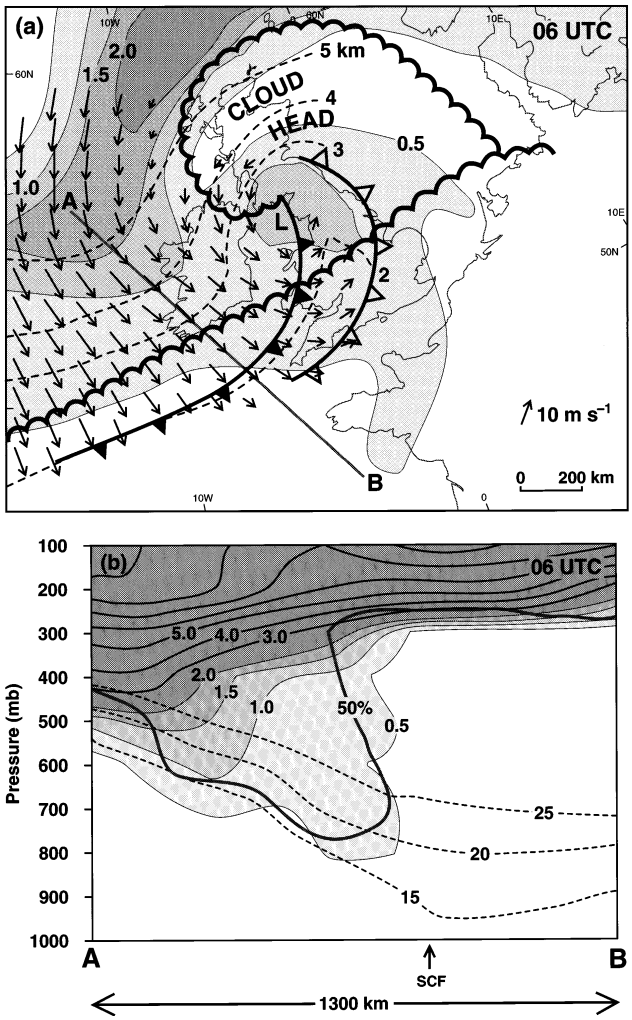

Figure 6. *Three-dimensional structure of the dry intrusion associated with a cyclone system at 0600 UTC, on 8 December 1994, derived from the 0000 UTC forecast run of the operational Met. Office Limited-Area Model.* (a) *Plan view showing the distribution of potential vorticity (solid curves and increasingly dark shading for PV > 0.5, 1.0, 1.5 and 2.0 PVU) and system-relative flow within the* $\theta = 20$ °C *isentropic surface, the height of which is given by dashed curves at 2, 3, 4 and 5 km. Also shown are the cold fronts and cloud outlines as in Figure 5.* (b) *Cross-section along AB in* (a) *showing the relationship of the dry intrusion to the PV distribution in the vertical. PV is depicted as in* (a). *The thick curve shows the downward protrusion of air with relative humidity less than 50%. The dashed curves show the 20° isentrope and isentropes 5° on either side. (After Browning & Roberts, 1996.)*

polewards from beneath the polar-front cloud band. Figure 6(*a*) depicts the system-relative flow on the 20 °C isentropic surface, which the cross-section in (*b*) shows to be in the middle of the dry intrusion. The dry intrusion is characterised by air with relatively high PV emanating from the region of a tropopause fold, although at the resolution of the Limited-Area Model most of the PV is between 0.5 and 2 PV units rather than exhibiting the values of greater than 2 PV units typical of stratospheric air. Within the limitations of the steady-state assumption, Figure 6(*a*) shows that the dry intrusion is part of a flow that is systematically descending towards the position of the surface cold front (SCF).

When a dry intrusion nears the SCF it can interact with the high θ_w WCB air ahead of it in two distinct ways, giving different frontal archetypes. The detailed analysis of Browning & Roberts (1996) for this case shows that the transition between the two archetypes occurred close to where the section AB crosses the front. Using terminology introduced by Bergeron (1937) and applied by Sansom (1951), the cold front was a kata-front to the northeast of AB and an ana-front to the southwest.

Sections normal to the SCF through idealised kata- and ana-cold fronts are sketched in Figures 7(*a*) and (*c*), respectively. In the ana-cold front most of the dry-intrusion air undercuts an extrusion of WCB air as part of a well-developed transverse circulation which generates a wide rainband behind the narrow cold-frontal rainband that is situated at the SCF. In the kata-cold front the dry-intrusion air overruns the SCF and WCB air for a distance that varies from tens to perhaps 200 kilometres; it then terminates as a UCF where the WCB deepens abruptly and often convectively (not shown in Figure 7(*a*)). This corresponds to the split cold-front model of Browning & Monk (1982). The split upper and surface cold fronts are plotted separately in the kata-cold frontal region of Figure 6(*a*). Kata- and ana-cold fronts are extremes in a spectrum of frontal structures. Figure 7(*b*) shows an intermediate structure corresponding to an early stage in the evolution of an ana-cold front from a kata-cold front.

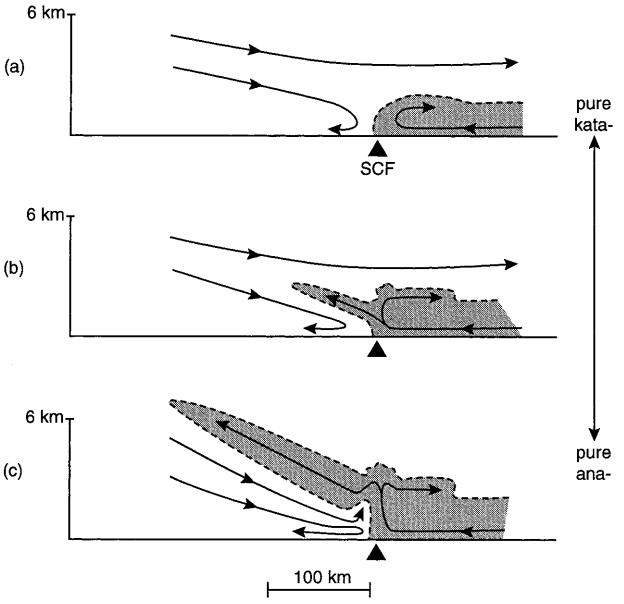

Figure 7. *Schematic cross-sectional representations of the spectrum of cold-front types, ranging from a pure kata-cold front* (a) *to a pure ana-cold front* (c). *Arrows show transverse flow relative to the front. Stippled shading bounded by dashed lines represents boundary-layer air or extruded boundary-layer air.*

4. Development of potential instability associated with dry intrusions

When a dry intrusion with its relatively low θ_w overruns secondary warm-conveyor-belt air at a kata-cold front, potential instability is generated. This may eventually be released as convection after sufficient lifting has occurred. The mode of development of the region of potential instability, and indeed the formation of the kata-cold front itself, can be visualised by considering the way in which the θ_w-field evolves during overrunning (Figure 8).

Figure 8 shows three snapshots from a mesoscale model run depicting the evolution of the θ_w-field during the deepening of a surface low (at location L). For simplicity a single θ_w-surface, corresponding to the middle of the frontal zone, is analysed where it intersects the 950 and 700 mb levels. The sequence shows how the surface winds up with time. This is associated with the field of rotation shown in the larger-area analysis on the right of Figure 8. The system-relative winds shown are for the 700 mb level where the rotation tends to be greatest. Lower down, the θ_w-surface rotates less, although it remains to be established to what extent this is due to differential rotation or to diabatic warming modifying θ_w closer to the ground. In any case, this kind of *effective* differential rotation with height is commonly observed and it leads to a localised region of overrunning. Figure 8 shows that the region of maximum overrunning coincides with the driest part of the dry intrusion.

Figure 9 shows a model-derived vertical section through the region of overrunning for a case in which severe thunderstorms were triggered. Dry-intrusion air with high PV can be seen (Figure 9(a)) slicing into a region of high relative humidity and cloud. The corresponding region is seen (in Figure 9(b)) to be associated with low θ_w air (equivalent potential temperature is plotted in the figure) overrunning high θ_w air in the boundary layer. The severe thunderstorms occurred at the leading edge of the dry intrusion where the model's convective parameterisation was in fact being activated, as shown by the column of asterisks in Figure 9(*b*).

5. Potential vorticity fine-structure within dry intrusions

In section 1 we discussed how part of a dry intrusion is likely to be characterised by high PV brought down from the upstream tropopause. In most cyclones

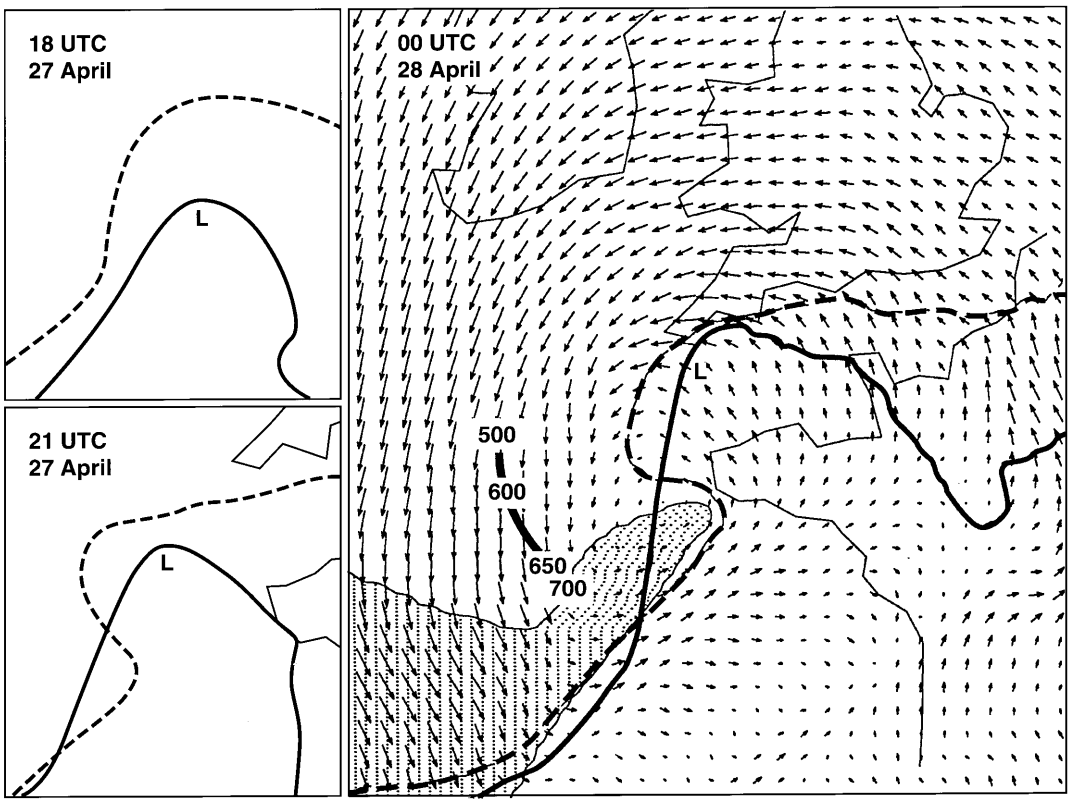

Figure 8. *Output from the Met. Office Mesoscale Model on 27/28 April 1992 depicting the winding up of the* $\theta_w = 9\,°C$ *surface under the influence of cyclonic rotation. Three-hourly sequence from 1800 UTC on 27 April (T+0) to 0000 UTC on 28 April (T+6).* Left side: *The 9 °C surface at 700 mb (dashed) and 950 mb (solid).* Right side: *System-relative flow and extent of dry air (relative humidity less than 30% shaded) at 700 mb superimposed on the* $\theta_w = 9\,°C$ *surface for 0000 UTC on 28 April. Numbers show positions of the axis of the maximum PV corresponding to the descending tropopause fold between the 500 and 700 mb levels. The main diagram is plotted to the same scale as those on the left-hand side but it covers a larger area. (After Browning* et al., *1997.)*

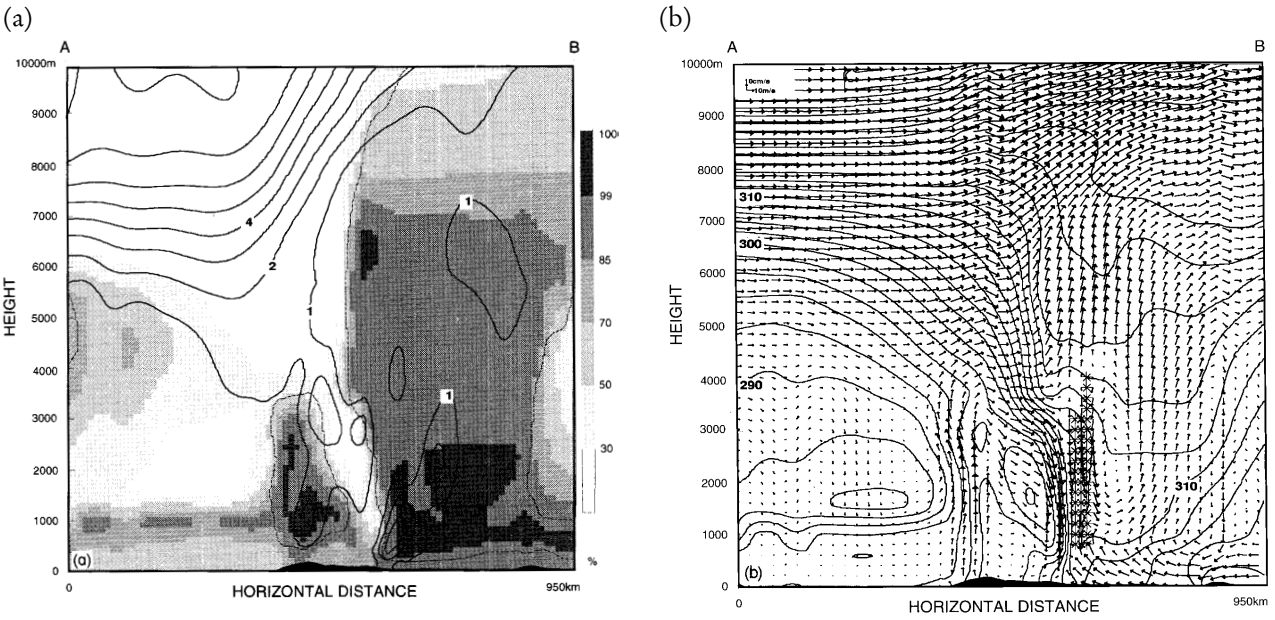

Figure 9. *Forecast cross-sections through a dry intrusion obtained from the Met. Office Mesoscale Model at 1800 UTC on 12 November 1991.* (a) *Relative humidity with respect to water (shading), the cloud boundary (dashed contours) and potential vorticity (solid contours at intervals of 1 PV unit).* (b) *Equivalent potential temperature (K) overlaid on the system-relative flow in the plane of the section. Regions experiencing parameterised release of potential instability are indicated by asterisks.*

stratospheric air descends a little but does not penetrate as far as the lower troposphere; however, occasionally, as in the case depicted in Figure 9, it actually reaches the boundary layer. Here it comes into close proximity with regions of high PV in the moist air, generated by latent heat release.

The question arises as to the dynamical significance of the stratospheric air descending to such low levels. A possible answer is provided by Figure 8 where the bold line connecting the numbers 500 to 700 marks the axis of the maximum PV corresponding to the descending tropopause fold. A mesoscale model cross-section (not depicted) shows that this was a thin filament, only 30 to 100 km wide, rather like that in Figure 9(*a*). It is evident from Figure 8 that the location of the PV filament does not coincide with the centre of rotation. Indeed, it may be that the filament is so small a feature that to a first approximation it can be considered to be passively advected within the dry-intrusion region by a circulation associated with the larger-scale PV distribution. The thin PV filament extends beneath a larger-scale downward bulge in the PV = 2 surface near 500 mb and it is likely that this is dynamically the more significant upper-level feature where cyclogenesis is concerned. WV imagery is highly responsive to dry air at such levels and above (Weldon & Holmes, 1991) and this, together with the association between high PV and low humidity in these regions, is what underpins the belief that WV imagery can be used as a proxy for identifying and bogussing errors in NWP model-derived PV (Demirtas, 1996).

6. Dry intrusions in the absence of strong low-level forcing

Dry intrusions are a manifestation of upper-level forcing of cyclogenesis associated with a positive upper-level PV anomaly (or upper-level trough, or jet streak, depending on one's point of view). Forcing of cyclogenesis can also occur at lower levels in association with PV anomalies within the moist air. In rapidly developing cyclones, upper-and lower-level effects tend to couple as the high-level PV-maximum overruns the low-level baroclinic zone (Hoskins *et al*., 1985). Often, however, strong upper-level forcing occurs in the absence of major low-level forcing or baroclinic zones. The result may be a relatively weak surface cyclone but the dry intrusion can still produce substantial overrunning and convective weather events, as shown in Figure 10.

Figure 10 is a three-hourly sequence of model analyses and Meteosat imagery during the development of a shallow surface low. The dry intrusion of interest was related to the blue area (dark zone) in the WV imagery (right-hand column) that travelled from southwest of Ireland to central England over the period shown. The dry intrusion was associated with an isolated PV anomaly which became cut off from an upper-level PV strip, but we have chosen to show instead the corresponding 500-mb absolute-vorticity maximum (blue area in left column), which intensified over the period due to vertical stretching. The match between the blue areas in the left and right columns is good but not perfect. The mismatch is due partly to model error and partly to the outbreak of convection leading to moistening and hence disappearance of part of the dry intru-

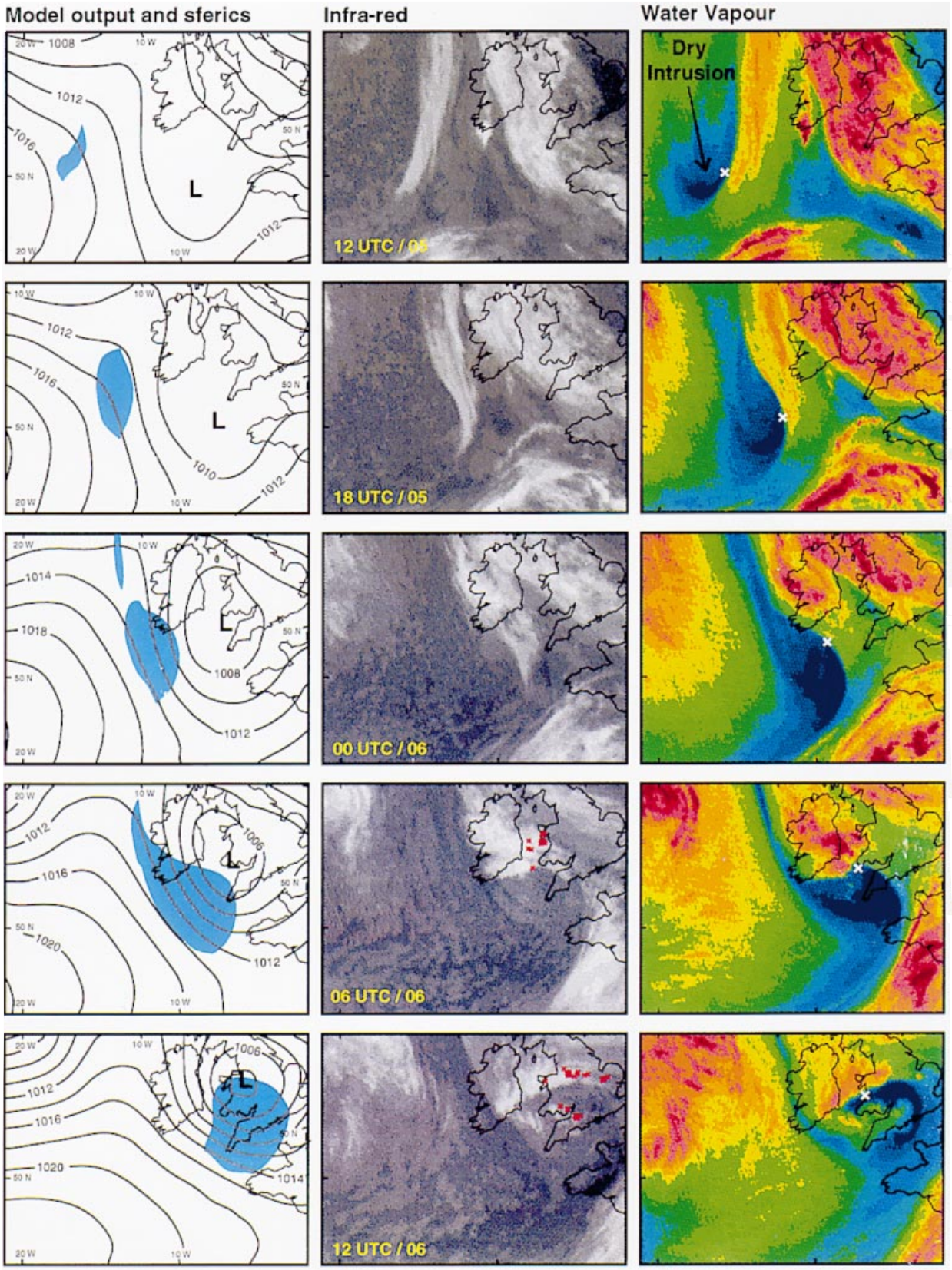

Figure 10. *Evolution of a thundery dry-intrusion event, from 1200 UTC on 5 August (top row) to 1200 UTC on 6 August 1996 (bottom row). Left column: Met Office Limited-Area Model analyses (contours represent mean sea-level pressure in mb; the blue area represents 500 mb absolute vorticity in excess of* 20×10^{-5} s^{-1}*). Middle column: Meteosat infra-red imagery (coldest clouds white) and sferics reports within ± 20 minutes of the analysis time (red crosses). Right column: Meteosat WV imagery (warm colours moist, cold colours dry). Times of the WV imagery are 30 minutes later than for the corresponding IR images. The white crosses in the right-hand column denote the centre of rotation of the leading edge of the dark zone (blue area) in the WV imagery as seen in action replay. (Courtesy of N. M. Roberts.)*

sion (especially at the later time over southwest Britain).

The infra-red imagery in the middle column of Figure 10 shows that there were two major cloud areas at the initial time. The band of cloud over England was associated with a broad surface trough. The smaller cloud band west of Ireland is the one that was associated with the main upper-level forcing; initially it was not accompanied by any surface-pressure feature but later it moved toward the surface low over Wales which then deepened by 5 mb in 18 hours. The point marked '×' in the right-hand column in Figure 10 corresponds to an apparent centre of rotation of the leading edge of the WV dark zone (blue area). This is seen most clearly when viewed in a system-relative animation.

Despite the weakness of the cyclogenesis at low levels, this was a major dry-intrusion event associated with strong upper-level vorticity: the model-derived peak absolute vorticity at 500 mb increased from 20 to 30 × 10^{-5} s^{-1} over the period and the overrunning led to heavy rain and thunderstorms (middle column). These storms went on to become extensive and heavy after the period shown in Figure 10. As is often the case, the thunderstorms developed in lines at the leading edge of the dry intrusion and also beneath the dry intrusion itself.

7. Conclusions

The identification of dry intrusions from WV imagery is useful in two ways for forecasting. First, it helps the forecaster understand what is happening on the mesoscale and to anticipate what may happen over the period of a nowcast. This is especially valuable in situations of rapid cyclogenesis and/or convective activity when local warnings of hazardous weather may need to be issued (Young, 1997). Secondly, it can be used to validate and bogus a NWP model. The bogussing can be quite effective because of the link between (parts of) dry intrusions and high PV. This may be done subjectively, as described by Mansfield (1994); current research at the Joint Centre for Mesoscale Meteorology (JCMM) is directed at automating this procedure.

References

Bader, M. J., Forbes, G. S., Grant, J. R., Lilley, R. B. E. & Waters, A. J. (1995). *Images in weather forecasting*. Cambridge University Press, 499 pp.

Bergeron, T. (1937). On the physics of fronts. *Bull. Am. Meteorol. Soc.*, **18:** 265–275.

Browning, K. A. & Golding, B. W. (1995). Mesoscale aspects of a dry intrusion within a vigorous cyclone, *Q. J. R. Meteorol. Soc.*, **121:** 463–493.

Browning, K. A. & Monk, G. A. (1982). A simple model for the synoptic analysis of cold fronts. *Q. J. R. Meteorol. Soc.*, **108:** 435–452.

Browning, K. A. & Roberts, N. M. (1994). Structure of a frontal cyclone. *Q. J. R. Meteorol. Soc.*, **120:** 1535–1557.

Browning, K. A. & Roberts, N. M. (1996). Variation of frontal and precipitation structure along a cold front. *Q. J. R. Meteorol. Soc.*, **122:** 1845–1872.

Browning, K. A., Clough, S. A., Davitt, C. S. A., Roberts, N. M., Hewson, T. D. & Healey, P. G. W. (1995). Observations of the mesoscale sub-structure in the cold air of a developing frontal cyclone. *Q. J. R. Meteorol. Soc.*, **121:** 1229–1254.

Browning, K. A., Ballard, S. P. & Davitt, C. S. A. (1997). High-resolution analysis of frontal fracture. *Mon. Wea. Rev.*, **125:** 1212–1230.

Danielsen, E. F. (1964). *Project Springfield Report*. Defense Atomic Support Agency, Washington D. C. 20301, DASA 1517 (NTIS # AD - 607980), 97 pp.

Demirtas, M. (1996). Sensitivity of short-range forecasts to local potential vorticity modifications, PhD Thesis, University of Reading, 227 pp.

Hewson, T. D. (1997). Objective verification of frontal wave cyclones. *Meteorol. Appl.*, **4:** 311–315.

Hoskins, B. J., McIntyre, M. E. & Robertson, A. W. (1985). On the use and significance of isentropic potential vorticity maps. *Q. J. R. Meteorol. Soc.,* **111:** 877–946.

Mansfield, D. (1994). The use of potential vorticity in forecasting cyclones: operational aspects. In *Proc. of Conference on the Life Cycles of Extratropical Cyclones. Vol III,* 27 June – 1 July 1994, Bergen, 326–331.

Sansom, H. W. (1951). A study of cold fronts over the British Isles. *Q. J. R. Meteorol. Soc.*, **77:** 96–120.

Shapiro, M. A. & Keyser, D. (1990). Fronts, jet streams and the tropopause. In *Extratropical cyclones. The Erik Palmén memorial volume.* Am. Meteorol. Soc., 167–191.

Smigielski, F. J. & Ellrod, G. P. (1985). Surface cyclogenesis as indicated by satellite imagery. In *NOAA Tech. Memo. NESDIS 9,* 1–29.

Thorncroft. C. D., Hoskins, B. J. & McIntyre, M. E. (1993). Two paradigms of baroclinic-wave life-cycle behaviour. *Q. J. R. Meteorol. Soc.*, **119:** 17–55.

Weldon, R. B. & Holmes, S. J. (1991). Water vapor imagery, interpretation and applications to weather analysis and forecasting. *NOAA Tech. Report NESDIS 57*, 213 pp.

Wernli, J. M. (1995). Lagrangian perspective of extratropical cyclogenesis, PhD Dissertation No. 11016, Swiss Federal Inst. of Tech., Zürich, 157 pp.

Young, M. V. (1994). A classification scheme for cyclone lifecycles : applications in analysis and short-period forecasting. In *Proc. of Conference on the Life Cycles of Extratropical Cyclones, Vol III, 27* June – 1 July 1994, Bergen, 380–385.

Young, M. V. (1997). Extratropical cyclones – a forecaster's perspective. *Meteorol. Appl.*, **4:** 293–300.

Young, M. V., Monk, G. A. & Browning, K. A. (1987). Interpretation of satellite imagery of a rapidly deepening cyclone. *Q. J. R. Meteorol. Soc.,* **113:** 1089–1115.